

Three-Jet Production in Deep-Inelastic Scattering at HERA

H1 Collaboration

Abstract

Three-jet production is studied for the first time in deep-inelastic positron-proton scattering. The measurement carried out with the H1 detector at HERA covers a large range of four-momentum transfer squared $5 < Q^2 < 5\,000\text{ GeV}^2$ and invariant three-jet masses $25 < M_{3\text{jet}} \lesssim 140\text{ GeV}$. Jets are defined by the inclusive k_\perp algorithm in the Breit frame. The size of the three-jet cross section and the ratio of the three-jet to the dijet cross section $R_{3/2}$ are described over the whole phase space by the predictions of perturbative QCD in next-to-leading order. The shapes of angular jet distributions deviate significantly from a uniform population of the available phase space but are well described by the QCD calculation.

To be submitted to Physics Letters

C. Adloff³³, V. Andreev²⁴, B. Andrieu²⁷, T. Anthonis⁴, V. Arkadov³⁵, A. Astvatsatourov³⁵, I. Ayyaz²⁸, A. Babaev²³, J. Bähr³⁵, P. Baranov²⁴, E. Barrelet²⁸, W. Bartel¹⁰, P. Bate²¹, A. Beglarian³⁴, O. Behnke¹³, C. Beier¹⁴, A. Belousov²⁴, T. Benisch¹⁰, Ch. Berger¹, T. Berndt¹⁴, J.C. Bizot²⁶, V. Boudry²⁷, W. Braunschweig¹, V. Brisson²⁶, H.-B. Bröker², D.P. Brown¹¹, W. Brückner¹², P. Bruel²⁷, D. Bruncko¹⁶, J. Bürger¹⁰, F.W. Büsser¹¹, A. Bunyatyan^{12,34}, H. Burkhardt¹⁴, A. Burrage¹⁸, G. Buschhorn²⁵, A.J. Campbell¹⁰, J. Cao²⁶, T. Carli²⁵, S. Caron¹, D. Clarke⁵, B. Clerbaux⁴, C. Collard⁴, J.G. Contreras^{7,41}, Y.R. Coppens³, J.A. Coughlan⁵, M.-C. Cousinou²², B.E. Cox²¹, G. Cozzika⁹, J. Cvach²⁹, J.B. Dainton¹⁸, W.D. Dau¹⁵, K. Daum^{33,39}, M. Davidsson²⁰, B. Delcourt²⁶, N. Delerue²², R. Demirchyan³⁴, A. De Roeck^{10,43}, E.A. De Wolf⁴, C. Diaconu²², J. Dingfelder¹³, P. Dixon¹⁹, V. Dodonov¹², J.D. Dowell³, A. Drouskoi²³, A. Dubak²⁵, C. Duprel², G. Eckerlin¹⁰, D. Eckstein³⁵, V. Efremenko²³, S. Egli³², R. Eichler³⁶, F. Eisele¹³, E. Eisenhandler¹⁹, M. Ellerbrock¹³, E. Elsen¹⁰, M. Erdmann^{10,40,e}, W. Erdmann³⁶, P.J.W. Faulkner³, L. Favart⁴, A. Fedotov²³, R. Felst¹⁰, J. Ferencei¹⁰, S. Ferron²⁷, M. Fleischer¹⁰, Y.H. Fleming³, G. Flügge², A. Fomenko²⁴, I. Foresti³⁷, J. Formánek³⁰, J.M. Foster²¹, G. Franke¹⁰, E. Gabathuler¹⁸, K. Gabathuler³², J. Garvey³, J. Gassner³², J. Gayler¹⁰, R. Gerhards¹⁰, C. Gerlich¹³, S. Ghazaryan³⁴, L. Goerlich⁶, N. Gogitidze²⁴, M. Goldberg²⁸, C. Goodwin³, C. Grab³⁶, H. Grässler², T. Greenshaw¹⁸, G. Grindhammer²⁵, T. Hadig¹³, D. Haidt¹⁰, L. Hajduk⁶, W.J. Haynes⁵, B. Heinemann¹⁸, G. Heinzelmann¹¹, A. Heister², R.C.W. Henderson¹⁷, S. Hengstmann³⁷, H. Henschel³⁵, R. Heremans⁴, G. Herrera^{7,41}, I. Herynek²⁹, M. Hildebrandt³⁷, M. Hilgers³⁶, K.H. Hiller³⁵, J. Hladký²⁹, P. Höting², D. Hoffmann²², R. Horisberger³², S. Hurling¹⁰, M. Ibbotson²¹, Ç. İşsever⁷, M. Jacquet²⁶, M. Jaffre²⁶, L. Janauschek²⁵, D.M. Jansen¹², X. Janssen⁴, V. Jemanov¹¹, L. Jönsson²⁰, D.P. Johnson⁴, M.A.S. Jones¹⁸, H. Jung^{20,10}, H.K. Kästli³⁶, D. Kant¹⁹, M. Kapichine⁸, M. Karlsson²⁰, O. Karschnick¹¹, F. Keil¹⁴, N. Keller³⁷, J. Kennedy¹⁸, I.R. Kenyon³, S. Kermiche²², C. Kiesling²⁵, P. Kjellberg²⁰, M. Klein³⁵, C. Kleinwort¹⁰, G. Knies¹⁰, B. Koblitz²⁵, S.D. Kolya²¹, V. Korbel¹⁰, P. Kostka³⁵, S.K. Kotelnikov²⁴, R. Koutouev¹², A. Koutov⁸, M.W. Krasny²⁸, H. Krehbiel¹⁰, J. Kroseberg³⁷, K. Krüger¹⁰, A. Küpper³³, T. Kuhr¹¹, T. Kurča^{25,16}, R. Lahmann¹⁰, D. Lamb³, M.P.J. Landon¹⁹, W. Lange³⁵, T. Laštovička³⁵, P. Laycock¹⁸, E. Lebailly²⁶, A. Lebedev²⁴, B. Leißner¹, R. Lemrani¹⁰, V. Lendermann⁷, S. Levonian¹⁰, M. Lindstroem²⁰, B. List³⁶, E. Lobodzinska^{10,6}, B. Lobodzinski^{6,10}, A. Loginov²³, N. Loktionova²⁴, V. Lubimov²³, S. Lüders³⁶, D. Lüke^{7,10}, L. Lytkin¹², N. Magnussen³³, H. Mahlke-Krüger¹⁰, N. Malden²¹, E. Malinovski²⁴, I. Malinovski²⁴, R. Maraček²⁵, P. Marage⁴, J. Marks¹³, R. Marshall²¹, H.-U. Martyn¹, J. Martyniak⁶, S.J. Maxfield¹⁸, D. Meer³⁶, A. Mehta¹⁸, K. Meier¹⁴, P. Merkel¹⁰, A.B. Meyer¹¹, H. Meyer³³, J. Meyer¹⁰, P.-O. Meyer², S. Mikocki⁶, D. Milstead¹⁸, T. Mkrtchyan³⁴, R. Mohr²⁵, S. Mohrdieck¹¹, M.N. Mondragon⁷, F. Moreau²⁷, A. Morozov⁸, J.V. Morris⁵, K. Müller³⁷, P. Murín^{16,42}, V. Nagovizin²³, B. Naroska¹¹, J. Naumann⁷, Th. Naumann³⁵, G. Nellen²⁵, P.R. Newman³, T.C. Nicholls⁵, F. Niebergall¹¹, C. Niebuhr¹⁰, O. Nix¹⁴, G. Nowak⁶, T. Nunnemann¹², J.E. Olsson¹⁰, D. Ozerov²³, V. Panassik⁸, C. Pascaud²⁶, G.D. Patel¹⁸, M. Peez²², E. Perez⁹, J.P. Phillips¹⁸, D. Pitzl¹⁰, R. Pöschl⁷, I. Potachnikova¹², B. Povh¹², K. Rabbertz¹, G. Rädcl¹, J. Rauschenberger¹¹, P. Reimer²⁹, B. Reisert²⁵, D. Reyna¹⁰, S. Riess¹¹, C. Risler²⁵, E. Rizvi³, P. Robmann³⁷, R. Roosen⁴, A. Rostovtsev²³, C. Royon⁹, S. Rusakov²⁴, K. Rybicki⁶, D.P.C. Sankey⁵, J. Scheins¹, F.-P. Schilling¹³, P. Schleper¹⁰, D. Schmidt³³, D. Schmidt¹⁰, S. Schmitt¹⁰, M. Schneider²², L. Schoeffel⁹, A. Schöning³⁶, T. Schörner²⁵, V. Schröder¹⁰, H.-C. Schultz-Coulon⁷, C. Schwanenberger¹⁰, K. Sedlák²⁹,

F. Sefkow³⁷, V. Shekelyan²⁵, I. Sheviakov²⁴, L.N. Shtarkov²⁴, Y. Sirois²⁷, T. Sloan¹⁷,
P. Smirnov²⁴, V. Solochenko^{23,†}, Y. Soloviev²⁴, V. Spaskov⁸, A. Specka²⁷, H. Spitzer¹¹,
R. Stamen⁷, J. Steinhart¹⁰, B. Stella³¹, A. Stellberger¹⁴, J. Stiewe¹⁴, U. Straumann³⁷,
W. Struczinski², M. Swart¹⁴, M. Taševský²⁹, V. Tchernyshov²³, S. Tchetchelnitski²³,
G. Thompson¹⁹, P.D. Thompson³, N. Tobien¹⁰, D. Traynor¹⁹, P. Truöl³⁷, G. Tsipolitis^{10,38},
I. Tsurin³⁵, J. Turnau⁶, J.E. Turney¹⁹, E. Tzamariudaki²⁵, S. Udluft²⁵, A. Usik²⁴, S. Valkár³⁰,
A. Valkárová³⁰, C. Vallée²², P. Van Mechelen⁴, S. Vassiliev⁸, Y. Vazdik²⁴, A. Vichnevski⁸,
K. Wacker⁷, R. Wallny³⁷, T. Walter³⁷, B. Waugh²¹, G. Weber¹¹, M. Weber¹⁴, D. Wegener⁷,
M. Werner¹³, N. Werner³⁷, G. White¹⁷, S. Wiesand³³, T. Wilksen¹⁰, M. Winde³⁵,
G.-G. Winter¹⁰, Ch. Wissing⁷, M. Wobisch², H. Wollatz¹⁰, E. Wünsch¹⁰, A.C. Wyatt²¹,
J. Žáček³⁰, J. Zálešák³⁰, Z. Zhang²⁶, A. Zhokin²³, F. Zomer²⁶, J. Zsembery⁹, and
M. zur Nedden¹⁰

¹ *I. Physikalisches Institut der RWTH, Aachen, Germany^a*

² *III. Physikalisches Institut der RWTH, Aachen, Germany^a*

³ *School of Physics and Space Research, University of Birmingham, Birmingham, UK^b*

⁴ *Inter-University Institute for High Energies ULB-VUB, Brussels; Universitaire Instelling Antwerpen, Wilrijk; Belgium^c*

⁵ *Rutherford Appleton Laboratory, Chilton, Didcot, UK^b*

⁶ *Institute for Nuclear Physics, Cracow, Poland^d*

⁷ *Institut für Physik, Universität Dortmund, Dortmund, Germany^a*

⁸ *Joint Institute for Nuclear Research, Dubna, Russia*

⁹ *CEA, DSM/DAPNIA, CE-Saclay, Gif-sur-Yvette, France*

¹⁰ *DESY, Hamburg, Germany*

¹¹ *II. Institut für Experimentalphysik, Universität Hamburg, Hamburg, Germany^a*

¹² *Max-Planck-Institut für Kernphysik, Heidelberg, Germany^a*

¹³ *Physikalisches Institut, Universität Heidelberg, Heidelberg, Germany^a*

¹⁴ *Kirchhoff-Institut für Physik, Universität Heidelberg, Heidelberg, Germany^a*

¹⁵ *Institut für experimentelle und Angewandte Physik, Universität Kiel, Kiel, Germany^a*

¹⁶ *Institute of Experimental Physics, Slovak Academy of Sciences, Košice, Slovak Republic^{e,f}*

¹⁷ *School of Physics and Chemistry, University of Lancaster, Lancaster, UK^b*

¹⁸ *Department of Physics, University of Liverpool, Liverpool, UK^b*

¹⁹ *Queen Mary and Westfield College, London, UK^b*

²⁰ *Physics Department, University of Lund, Lund, Sweden^g*

²¹ *Physics Department, University of Manchester, Manchester, UK^b*

²² *CPPM, CNRS/IN2P3 - Univ Mediterranee, Marseille - France*

²³ *Institute for Theoretical and Experimental Physics, Moscow, Russia*

²⁴ *Lebedev Physical Institute, Moscow, Russia^{e,h}*

²⁵ *Max-Planck-Institut für Physik, München, Germany^a*

²⁶ *LAL, Université de Paris-Sud, IN2P3-CNRS, Orsay, France*

²⁷ *LPNHE, Ecole Polytechnique, IN2P3-CNRS, Palaiseau, France*

²⁸ *LPNHE, Universités Paris VI and VII, IN2P3-CNRS, Paris, France*

²⁹ *Institute of Physics, Academy of Sciences of the Czech Republic, Praha, Czech Republic^{e,i}*

³⁰ *Faculty of Mathematics and Physics, Charles University, Praha, Czech Republic^{e,i}*

³¹ *Dipartimento di Fisica Università di Roma Tre and INFN Roma 3, Roma, Italy*

³² *Paul Scherrer Institut, Villigen, Switzerland*

³³ *Fachbereich Physik, Bergische Universität Gesamthochschule Wuppertal, Wuppertal, Germany^a*

³⁴ *Yerevan Physics Institute, Yerevan, Armenia*

³⁵ *DESY, Zeuthen, Germany^a*

³⁶ *Institut für Teilchenphysik, ETH, Zürich, Switzerland^j*

³⁷ *Physik-Institut der Universität Zürich, Zürich, Switzerland^j*

³⁸ *Also at Physics Department, National Technical University, Zografou Campus, GR-15773 Athens, Greece*

³⁹ *Also at Rechenzentrum, Bergische Universität Gesamthochschule Wuppertal, Germany*

⁴⁰ *Also at Institut für Experimentelle Kernphysik, Universität Karlsruhe, Karlsruhe, Germany*

⁴¹ *Also at Dept. Fis. Ap. CINVESTAV, Mérida, Yucatán, México^k*

⁴² *Also at University of P.J. Šafárik, Košice, Slovak Republic*

⁴³ *Also at CERN, Geneva, Switzerland*

[†] *Deceased*

^a *Supported by the Bundesministerium für Bildung, Wissenschaft, Forschung und Technologie, FRG, under contract numbers 7AC17P, 7AC47P, 7DO55P, 7HH17I, 7HH27P, 7HD17P, 7HD27P, 7KI17I, 6MP17I and 7WT87P*

^b *Supported by the UK Particle Physics and Astronomy Research Council, and formerly by the UK Science and Engineering Research Council*

^c *Supported by FNRS-NFWO, IISN-IKW*

^d *Partially Supported by the Polish State Committee for Scientific Research, grant no. 2P0310318 and SPUB/DESY/P03/DZ-1/99, and by the German Federal Ministry of Education and Science, Research and Technology (BMBF)*

^e *Supported by the Deutsche Forschungsgemeinschaft*

^f *Supported by VEGA SR grant no. 2/5167/98*

^g *Supported by the Swedish Natural Science Research Council*

^h *Supported by Russian Foundation for Basic Research grant no. 96-02-00019*

ⁱ *Supported by the Ministry of Education of the Czech Republic under the projects INGO-LA116/2000 and LN00A006, and by GA AVČR grant no B1010005*

^j *Supported by the Swiss National Science Foundation*

^k *Supported by CONACyT*

1 Introduction

Multi-jet production in deep-inelastic scattering (DIS) has been successfully used at HERA to test the predictions of perturbative QCD (pQCD) over a large range of four-momentum transfer squared Q^2 [1]. Recently the H1 collaboration has determined the strong coupling constant α_s and the gluon density in the proton [2] from the inclusive jet and the dijet cross sections measured in the Breit frame. While these cross sections are directly sensitive to QCD effects of order $\mathcal{O}(\alpha_s)$, the three-jet cross section in DIS is already proportional to α_s^2 in leading order in pQCD. The higher sensitivity to α_s and the greater number of degrees of freedom of the three-jet final state thus allow the QCD predictions to be tested in more detail in three-jet production. In this paper we present for the first time differential measurements of the three-jet cross section in neutral current DIS and measurements of shapes of angular jet distributions which are sensitive to dynamic effects of the interaction. Similar studies of three-jet production in reactions with initial state hadrons have been carried out previously in hadron-hadron collisions at the SPS [3], the ISR [4] and at the TEVATRON [5] as well as in photoproduction at HERA [6]. The present analysis includes the first comparison of three-jet distributions measured in hadron induced reactions with a perturbative QCD calculation in next-to-leading order α_s [7].

In neutral current DIS the lepton interacts with a parton in the proton via the exchange of a boson (γ , Z). At a fixed center-of-mass energy the kinematics of the lepton inclusive reaction (for unpolarized lepton and proton beams) is given by two variables which are here chosen to be the four-momentum transfer squared Q^2 and the Bjorken scaling variable x_{Bj} . The subprocess $1 + 2 \rightarrow 3 + 4 + 5$ in which three massless jets emerge from the boson-parton reaction is fully described by six further variables which can be constructed from the energies E_i and the momenta \vec{p}_i of the jets in the three-jet center-of-mass (CM) frame. It is convenient to label the three jets ($i = 3, 4, 5$) in the order of decreasing energies in the three-jet CM frame. These variables are conventionally chosen [8] to be the azimuthal orientation of the three-jet system, the invariant mass of the three-jet system $M_{3\text{jet}}$, the jet energy fractions¹ X_3 , X_4

$$X_3 \equiv \frac{2 E_3}{M_{3\text{jet}}}, \quad X_4 \equiv \frac{2 E_4}{M_{3\text{jet}}}, \quad (1)$$

and two angles θ_3 and ψ_3 that specify the relative orientation of the jets,

$$\cos \theta_3 \equiv \frac{\vec{p}_B \cdot \vec{p}_3}{|\vec{p}_B| |\vec{p}_3|}, \quad \cos \psi_3 \equiv \frac{(\vec{p}_3 \times \vec{p}_B) \cdot (\vec{p}_4 \times \vec{p}_5)}{|\vec{p}_3 \times \vec{p}_B| |\vec{p}_4 \times \vec{p}_5|}, \quad (2)$$

where \vec{p}_B denotes the direction of the proton beam. As indicated in Fig. 1, θ_3 is the angle of the highest energetic jet with respect to the proton beam direction and ψ_3 is the angle between the plane spanned by the highest energy jet and the proton beam and the plane containing the three jets. The angle ψ_3 indicates whether the third jet (i.e. the lowest energy jet) is radiated within ($\psi_3 \rightarrow 0$ or $\psi_3 \rightarrow \pi$) or up to perpendicular to ($\psi_3 \rightarrow \pi/2$) the plane containing the highest energy jet and the proton beam. In dijet production, in the dijet center-of-mass frame both jets carry half of the available energy and are scattered back-to-back. The presence of a third jet, however, allows the $\cos \theta_3$ distribution to be asymmetric in the three-jet CM frame

¹Note that from energy and momentum conservation $X_3 + X_4 + X_5 = 2$ with $X_5 = (2 E_5)/M_{3\text{jet}}$.

and the energies of the two leading jets to be smaller than half of the total available energy ($X_3, X_4 < 1$).

The observable $R_{3/2}$, defined by the ratio of the inclusive three-jet cross section and the inclusive two-jet cross section, is of interest especially for quantitative studies, since in this ratio both experimental and some theoretical uncertainties cancel to a large extent.

This paper presents measurements of the inclusive three-jet cross section in DIS as a function of Q^2 , x_{Bj} and $M_{3\text{jet}}$. Distributions of three-jet events are measured in the variables X_3 , X_4 , $\cos \theta_3$ and ψ_3 and are normalized to the integrated three-jet cross section. The ratio $R_{3/2}$ is measured as a function of Q^2 . The kinematic range of the analysis covers four-momentum transfers squared Q^2 between 5 GeV² and 5000 GeV² and invariant three-jet masses $M_{3\text{jet}}$ in the range from 25 GeV to 140 GeV.

2 Event Selection

The analysis is based on data taken in positron-proton collisions with the H1 detector at HERA in the years 1995–1997 with a positron beam energy of $E_e = 27.5$ GeV and a proton beam energy of $E_p = 820$ GeV, leading to a center-of-mass energy \sqrt{s} of 300 GeV. A detailed description of the H1 detector can be found in [9]. The main detector components relevant for the present analysis are the liquid argon (LAr) calorimeter [10], the backward lead-fiber calorimeter (SpaCal) [11] and the tracking chamber system. In the polar angular² range $4^\circ < \theta < 154^\circ$ ($153^\circ < \theta < 177^\circ$) the electromagnetic and hadronic energies are measured by the LAr calorimeter (SpaCal) with full azimuthal coverage. Charged particle tracks are measured in two concentric drift chamber modules ($25^\circ < \theta < 165^\circ$) and by a forward tracking detector ($7^\circ < \theta < 25^\circ$).

The experimental procedure is similar to the one used in a previous measurement of the inclusive jet and the dijet cross section [2]. Here we briefly summarize only the salient features. The identification and triggering of neutral current DIS events is based on the reconstruction of the event vertex and the detection of the scattered positron as a compact electromagnetic cluster in either the SpaCal (“low Q^2 ”) or the LAr calorimeter (“high Q^2 ”). The two event samples correspond to integrated luminosities of $\mathcal{L}_{\text{int}} = 21.1 \text{ pb}^{-1}$ (low Q^2) and $\mathcal{L}_{\text{int}} = 32.9 \text{ pb}^{-1}$ (high Q^2), respectively. The trigger efficiencies for the final jet event samples are above 98%. The hadronic final state is reconstructed from a combination of tracks with low transverse momentum ($p_T < 2 \text{ GeV}$) and energy deposits in the LAr calorimeter and the SpaCal. The kinematic variables Q^2 , x_{Bj} and $y = Q^2/(s x_{\text{Bj}})$ are reconstructed using the $e\Sigma$ -method [12]. The kinematic range of the analysis is specified by

$$\begin{aligned} \text{low } Q^2: & \quad 5 < Q^2 < 100 \text{ GeV}^2 \quad \text{and} \quad \theta_{\text{positron}} > 156^\circ, \\ \text{high } Q^2: & \quad 150 < Q^2 < 5000 \text{ GeV}^2, \\ \text{low } Q^2 \text{ and high } Q^2: & \quad 0.2 < y < 0.6. \end{aligned} \tag{3}$$

²The polar angle θ is defined with respect to the positive z -axis which is given by the proton beam direction in all reference frames.

The jet selection is carried out in the Breit frame in which $\vec{q} + 2x_{\text{Bj}}\vec{P} = 0$, where \vec{q} and \vec{P} are the momenta of the exchanged boson and of the incoming proton, respectively. Jets are defined by the inclusive k_{\perp} clustering algorithm [13] which is applied to the final state particles, excluding the scattered positron. The parameter R_0 , which defines the minimal separation of jets in pseudorapidity³ and azimuth space, is set to $R_0 = 1$. The clustering of particles is done in the E_T recombination scheme in which the resulting jets are massless. A detailed description of the procedure is given in [14]. The jet phase space is defined by cuts on the jet pseudorapidity $\eta_{\text{jet,lab}}$ in the laboratory frame and on the transverse jet energy E_T in the Breit frame

$$-1 < \eta_{\text{jet,lab}} < 2.5 \quad \text{and} \quad E_T > 5 \text{ GeV}. \quad (4)$$

The inclusive three-jet (dijet) sample consists of all events with three (two) or more jets from which the three (two) jets of highest E_T have an invariant mass of

$$M_{3\text{jet}} > 25 \text{ GeV} \quad (M_{2\text{jet}} > 25 \text{ GeV}). \quad (5)$$

With these selection criteria applied, the inclusive three-jet event sample at low Q^2 (high Q^2) contains 2903 (666) events, and the corresponding inclusive dijet sample contains 6746 (2005) events. The jet selection cuts in (4) deplete the phase space regions of $\cos \theta_3 \rightarrow \pm 1$, $\psi_3 \rightarrow 0$ and $\psi_3 \rightarrow \pi$ [15]. To reduce this influence the following additional cuts are applied for the measurement of the differential distributions of the variables X_3 , X_4 , $\cos \theta_3$ and ψ_3

$$\begin{aligned} X_3 &< 0.95, \\ |\cos \theta_3| &< 0.8, \\ M_{3\text{jet}} &> 40 \text{ GeV} \quad \text{only for } Q^2 < 100 \text{ GeV}^2. \end{aligned} \quad (6)$$

Due to the limited size of the event sample the last cut is not applied in the high Q^2 analysis. The cuts in (6) are passed by 523 (536) three-jet events in the low Q^2 (high Q^2) event sample. The size of the photoproduction background has been estimated using two samples of photoproduction events generated by PYTHIA [16] and PHOJET [17] and is found to be negligible (i.e. below 2%) in all distributions measured.

3 Correction of the Data

The data are corrected for effects of detector resolution and acceptance, as well as for inefficiencies of the selection and for higher order QED effects. The correction functions are determined using event samples generated by the Monte Carlo event generators LEPTO [18], RAPGAP [19] and ARIADNE [20], all interfaced to HERACLES [21] to take QED corrections into account. For each generator two event samples are generated. The first sample, which includes QED corrections, is subjected to a detailed simulation of the H1 detector based on GEANT [22]. The second event sample is generated under the same physics assumptions, but without QED corrections and without detector simulation. The correction functions are determined bin-wise for each observable as the ratio of its value in the second sample and its value in the first sample.

³The pseudorapidity η is related to the polar angle θ by $\eta = -\ln(\tan \theta/2)$.

The applicability of the simulated event samples for the correction procedure has been tested by comparing a variety of their distributions to the data for the three-jet and the dijet event samples [15]. The simulated events are found to give a good description of single jet related quantities such as the surrounding energy flow, their angular distributions and their internal structure. Based on the event simulation the bin widths of all variables have been adjusted to match their resolution. At low Q^2 (high Q^2) the correction functions are determined using event samples from RAPGAP and ARIADNE (LEPTO and ARIADNE). In both Q^2 regions the correction functions agree within typically 10% for the measured cross sections and for the ratio $R_{3/2}$ and within typically 5% for the normalized distributions of X_3 , X_4 , $\cos\theta_3$ and ψ_3 . The final correction functions are taken to be the average of the two models and half of their difference is used as an estimate of the model dependence. The list of further experimental uncertainties considered in the analysis is identical to the one in the recent measurement of inclusive jet and dijet cross sections [2]. The uncertainty of the measured cross sections are typically 16% and are dominated by systematic effects, the largest contributions being due to the hadronic energy scale of the LAr calorimeter and the model dependence of the correction functions. The uncertainties of the measured rate $R_{3/2}$ have equal statistical and systematic contributions while in the normalized distributions the statistical uncertainties dominate.

4 Results

The measured three-jet distributions are presented in Figs. 2–5 and in table 1. The inner error bars represent the statistical uncertainties and the outer error bars the quadratic sum of all uncertainties. The data are compared to the pQCD predictions in leading order (LO) and in next-to-leading order (NLO) with and without hadronization corrections. The LO and NLO calculations are carried out in the $\overline{\text{MS}}$ -scheme for five massless quark flavors using the recent program NLOJET [7]. It was checked that the LO calculations from NLOJET agree with those of MEPJET [23] and DISENT [24]. Heavy quark mass effects are estimated using the LO calculation MEPJET and are found to lower the three-jet cross section by typically 5% at low Q^2 and 3% at high Q^2 . Renormalization and factorization scales (μ_r , μ_f) are set to the average transverse energy \overline{E}_T of the three jets in the Breit frame. The parton density functions of the proton are taken from the parameterization CTEQ5M1 [25]. The strong coupling constant is set to the world average value of $\alpha_s(M_Z) = 0.118$ [26] and is evolved according to the two-loop solution of the renormalization group equation. Hadronization corrections δ_{hadr} are determined using LEPTO as the relative change of an observable before and after hadronization. These corrections are in the range $-22\% < \delta_{\text{hadr}} < -18\%$ for the three-jet cross section and $-18\% < \delta_{\text{hadr}} < -10\%$ for the ratio $R_{3/2}$ over the whole range of Q^2 and they agree with those obtained from HERWIG [27] to within 2%. Hadronization corrections are negligible for the normalized distributions (Figs. 4 and 5) since they basically change the size of the three-jet cross section but not the shapes of differential distributions.

The three-jet cross section is presented in Fig. 2 (a) as a function of the four-momentum transfer squared Q^2 . The data are compared to the LO and NLO predictions, the latter with and without hadronization corrections. In the lower part of the figure the ratio of the measured cross section and the NLO prediction (corrected for hadronization effects) is shown. Over the whole range of Q^2 the NLO prediction (corrected for hadronization effects) gives a good description

of the data — at high Q^2 , where NLO corrections are small, but also at low Q^2 where the NLO prediction is a factor of two above the LO prediction. The theoretical prediction is subject to several uncertainties, the dominant sources being the value of the strong coupling constant, the parton density functions of the proton (especially the gluon density) and the renormalization scale dependence of the NLO calculation. In the lower part of Fig. 2 (a) the size of these uncertainties is displayed by three different bands, indicating variations of the strong coupling constant (by $\Delta\alpha_s(M_Z) = \pm 0.006$), the gluon density⁴ (overall by $\Delta g(x, \mu_f) = \pm 15\%$) and the renormalization scale (by $0.5 < (\mu_r/\bar{E}_T) < 2$). While at $Q^2 \gtrsim 50 \text{ GeV}^2$ the variation of α_s gives the largest effect, the renormalization scale dependence is the dominant source of uncertainty at lower values of Q^2 , i.e. in the region where NLO corrections are also large. Over the whole Q^2 range the change of the cross section, induced by the variation of the gluon density is approximately half as large as the change induced by the α_s variation.

For the ratio $R_{3/2}$ of the inclusive three-jet cross section and the inclusive dijet cross section which is shown in Fig. 2 (b) some experimental and theoretical uncertainties cancel. The data are measured as a function of Q^2 and compared to LO and NLO calculations which are corrected for hadronization effects. While the LO calculation predicts a stronger Q^2 dependence of $R_{3/2}$ than observed in the data, the NLO calculation gives a good description of the data over the whole range of Q^2 . Uncertainties in the theoretical prediction for the ratio $R_{3/2}(Q^2)$ are investigated in the same way as for the three-jet cross section. The NLO corrections for the three-jet and the dijet cross sections are of similar size. At low Q^2 this leads to a smaller NLO correction and renormalization scale dependence for the ratio $R_{3/2}$ than for the cross section. Furthermore, when measured in the same region of x_{Bj} and Q^2 , with the same cut on the invariant multi-jet mass, the three-jet and the dijet cross sections probe the parton density functions of the proton in the same range of proton momentum fractions $\xi = x_{\text{Bj}}(1 + M_{\text{n-jet}}^2/Q^2)$. Since both jet cross sections are dominated by gluon induced processes, the ratio $R_{3/2}$ is almost insensitive to variations of the gluon density in the proton. It is recognized that the ratio $R_{3/2}$ is experimentally measured and theoretically calculated with small uncertainties over the entire range of Q^2 . For the central value of $\alpha_s(M_Z) \approx 0.118$ used in the calculations, the theoretical predictions are consistent with the data for the three-jet cross section and the ratio $R_{3/2}$.

The three-jet cross section is displayed in Fig. 3 as a function of the Bjorken scaling variable x_{Bj} and the invariant three-jet mass $M_{3\text{jet}}$ over the range of $10^{-4} < x_{\text{Bj}} < 0.2$ and $25 < M_{3\text{jet}} < 140 \text{ GeV}$ in two regions of Q^2 . In the low Q^2 region the LO calculation underestimates the cross section at small x_{Bj} and small $M_{3\text{jet}}$ by a factor of two. The NLO calculation, however, gives a good description of the data.

In Fig. 4 the distributions of the energy fractions X_3 and X_4 of the two higher energetic jets are shown. They are normalized to the total three-jet cross section in the same kinematic range. The data are well described by the QCD prediction in NLO. For these normalized distributions NLO corrections are negligible and the LO calculation (not shown) can not be distinguished from the NLO curves. In addition the figures also include a three-jet distribution generated with a uniform population of the available three-body phase space (labeled “Phase Space”)⁵.

⁴The variations of $\alpha_s(M_Z)$ and the gluon density in the proton correspond roughly to the uncertainties within which both have been determined in a previous analysis [2] from jet cross sections in DIS.

⁵The phase space distribution of the three jets is generated according to the observed invariant mass spectrum using the jet separation and selection criteria as applied in the data. To apply the pseudorapidity cuts on the jets in

The phase space prediction is, however, similar to the NLO prediction, except for a small shift towards larger values of X_3 and X_4 , indicating the Bremsstrahlung nature of the process.

The normalized distributions of the angular variables $\cos \theta_3$ and ψ_3 are shown in Fig. 5 for the data at low Q^2 (left) and at high Q^2 (right). The $\cos \theta_3$ distributions in both Q^2 regions are peaked at the cut value of $\cos \theta_3 = \pm 0.8$, corresponding to angles close to the proton and the photon direction. The phase space prediction shows the opposite behavior, peaking at zero and falling towards $\cos \theta_3 \rightarrow \pm 0.8$. The QCD calculation in NLO shows an asymmetry around zero and gives a reasonable description of the effects seen in the data. The latter is also the case for the measured ψ_3 distributions which are relatively flat, while the underlying phase space is strongly peaked at $\psi_3 = \pi/2$. Although at low Q^2 the NLO prediction is almost a factor of two higher than the LO prediction, the shapes of the angular jet distributions are almost unaffected by the NLO correction. Differences between the QCD calculation and the phase space prediction indicate that due to the Bremsstrahlung nature of the process configurations are preferred in which the plane containing the two less energetic jets coincides with the plane spanned by the proton beam and the highest energetic jet, corresponding to values of $\psi_3 \rightarrow 0$ and $\psi_3 \rightarrow \pi$. These results are in qualitative agreement with measurements in $\bar{p}p$ collisions [3,5] and in γp collisions [6]. Differences in the observed shapes of the two variables at low and at high Q^2 are, to some extent, due to the phase space resulting from the different cuts in $M_{3\text{jet}}$.

5 Summary

A measurement of the three-jet cross section in deep-inelastic scattering has been presented. At a positron-proton center-of-mass energy \sqrt{s} of 300 GeV the production rates and angular distributions of three-jet events, selected in the Breit frame with $E_T > 5$ GeV, have been studied over a large range of four-momentum transfer squared, $5 < Q^2 < 5\,000$ GeV².

The inclusive three-jet cross section has been measured as a function of Q^2 , Bjorken- x and the invariant three-jet mass for invariant three-jet masses above 25 GeV. The ratio $R_{3/2}$ of the inclusive three-jet and the inclusive dijet cross section has been measured as a function of Q^2 . The predictions of perturbative QCD in next-to-leading order give a good description of the three-jet cross section and the ratio $R_{3/2}$ over the whole range of Q^2 for values of the strong coupling constant close to the current world average of $\alpha_s(M_Z) \simeq 0.118$. Angular jet distributions and jet energy fractions have been measured in the three-jet center-of-mass frame. The angular orientation of the three-jet system follows the radiation pattern expected from perturbative QCD. While the angular distributions are not consistent with a uniform population of the available phase space, they are reasonably well described by the QCD predictions.

Acknowledgments

We thank Erwin Mirkes, Zoltan Nagy, Mike H. Seymour and Dieter Zeppenfeld for many helpful discussions. We are grateful to the HERA machine group whose outstanding efforts have

the laboratory frame also the distributions of the variables Q^2 and x_{Bj} (which define the boost vector) are fitted to the data.

made and continue to make this experiment possible. We thank the engineers and technicians for their work in constructing and now maintaining the H1 detector, our funding agencies for financial support, the DESY technical staff for continual assistance and the DESY directorate for the hospitality which they extend to the non-DESY members of the collaboration.

References

- [1] C. Adloff *et al.* [H1 Collaboration], Eur. Phys. J. C **19** (2001) 429 [hep-ex/0010016];
C. Adloff *et al.* [H1 Collaboration], Eur. Phys. J. C **13** (2000) 415 [hep-ex/9806029];
C. Adloff *et al.* [H1 Collaboration], Eur. Phys. J. C **6** (1999) 575 [hep-ex/9807019];
C. Adloff *et al.* [H1 Collaboration], Eur. Phys. J. C **5** (1998) 625 [hep-ex/9806028];
J. Breitweg *et al.* [ZEUS Collaboration], Phys. Lett. B **507** (2001) 70 [hep-ex/0102042];
M. Derrick *et al.* [ZEUS Collaboration], Phys. Lett. B **363** (1995) 201 [hep-ex/9510001].
- [2] C. Adloff *et al.* [H1 Collaboration], Eur. Phys. J. C **19** (2001) 289 [hep-ex/0010054].
- [3] G. Arnison *et al.* [UA1 Collaboration], Phys. Lett. B **158** (1985) 494;
J. A. Appel *et al.* [UA2 Collaboration], Z. Phys. C **30** (1986) 341.
- [4] A. L. Angelis *et al.* [CMOR Collaboration], Nucl. Phys. B **303** (1988) 569;
T. Akesson *et al.* [Axial Field Spectrometer Collaboration], Z. Phys. C **32** (1986) 317.
- [5] B. Abbott *et al.* [D0 Collaboration], Phys. Rev. Lett. **86** (2001) 1955 [hep-ex/0009012];
S. Abachi *et al.* [D0 Collaboration], Phys. Rev. D **53** (1996) 6000 [hep-ex/9509005];
F. Abe *et al.* [CDF Collaboration], Phys. Rev. D **54** (1996) 4221 [hep-ex/9605004];
F. Abe *et al.* [CDF Collaboration], Phys. Rev. Lett. **75** (1995) 608;
F. Abe *et al.* [CDF Collaboration], Phys. Rev. D **45** (1992) 1448.
- [6] J. Breitweg *et al.* [ZEUS Collaboration], Phys. Lett. B **443** (1998) 394 [hep-ex/9810046].
- [7] Z. Nagy and Z. Trocsanyi, hep-ph/0104315.
- [8] S. Geer and T. Asakawa, Phys. Rev. D **53** (1996) 4793 [hep-ph/9510351].
- [9] I. Abt *et al.* [H1 Collaboration], Nucl. Instrum. Meth. A **386** (1997) 310.
- [10] B. Andrieu *et al.* [H1 Calorimeter Group Collaboration], Nucl. Instrum. Meth. A **336** (1993) 460;
B. Andrieu *et al.* [H1 Calorimeter Group Collaboration], Nucl. Instrum. Meth. A **336** (1993) 499;
B. Andrieu *et al.* [H1 Calorimeter Group Collaboration], Nucl. Instrum. Meth. A **350** (1994) 57.
- [11] R. D. Appuhn *et al.* [H1 SPACAL Group Collaboration], Nucl. Instrum. Meth. A **386** (1997) 397.
- [12] U. Bassler and G. Bernardi, Nucl. Instrum. Meth. A **426** (1999) 583 [hep-ex/9801017].

- [13] S. D. Ellis and D. E. Soper, Phys. Rev. D **48** (1993) 3160 [hep-ph/9305266];
S. Catani, Y. L. Dokshitzer, M. H. Seymour and B. R. Webber, Nucl. Phys. B **406** (1993) 187.
- [14] C. Adloff *et al.* [H1 Collaboration], Nucl. Phys. B **545** (1999) 3 [hep-ex/9901010].
- [15] A. Heister, Diploma Thesis, RWTH Aachen, Germany (1999);
R. Mohr, Phd Thesis, University of Hamburg, Germany, MPI-PhE/00-06 (2000).
- [16] H. Bengtsson and T. Sjöstrand, Comput. Phys. Commun. **46** (1987) 43 (version used: 5.7).
- [17] R. Engel, Z. Phys. C **66** (1995) 203 (version used: 1.03);
R. Engel and J. Ranft, Phys. Rev. D **54** (1996) 4244 [hep-ph/9509373].
- [18] G. Ingelman, A. Edin and J. Rathsman, Comput. Phys. Commun. **101** (1997) 108 [hep-ph/9605286] (version used: 6.5).
- [19] H. Jung, Comput. Phys. Commun. **86** (1995) 147 (version used: 2.08).
- [20] L. Lönnblad, Comput. Phys. Commun. **71** (1992) 15 (version used: 4.08).
- [21] A. Kwiatkowski, H. Spiesberger and H. J. Möhring, Comput. Phys. Commun. **69** (1992) 155.
- [22] CERN, GEANT, detector description and simulation tool, CERN Program Library Long Writeup W 5013 (1994).
- [23] E. Mirkes and D. Zeppenfeld, Phys. Lett. B **380** (1996) 205 [hep-ph/9511448].
- [24] S. Catani and M. H. Seymour, Nucl. Phys. B **485** (1997) 291 [Erratum-ibid. B **510** (1997) 503] [hep-ph/9605323].
- [25] H. L. Lai *et al.* [CTEQ Collaboration], Eur. Phys. J. C **12** (2000) 375 [hep-ph/9903282].
- [26] S. Bethke, J. Phys. G **G26** (2000) R27 [hep-ex/0004021];
D. E. Groom *et al.* [Particle Data Group Collaboration], Eur. Phys. J. C **15** (2000) 1.
- [27] G. Marchesini, B. R. Webber, G. Abbiendi, I. G. Knowles, M. H. Seymour and L. Stanco, Comput. Phys. Commun. **67** (1992) 465 (version used: 5.9).

three-jet center-of-mass frame:

$$1 + 2 \rightarrow 3 + 4 + 5$$

$$E_3 > E_4 > E_5$$

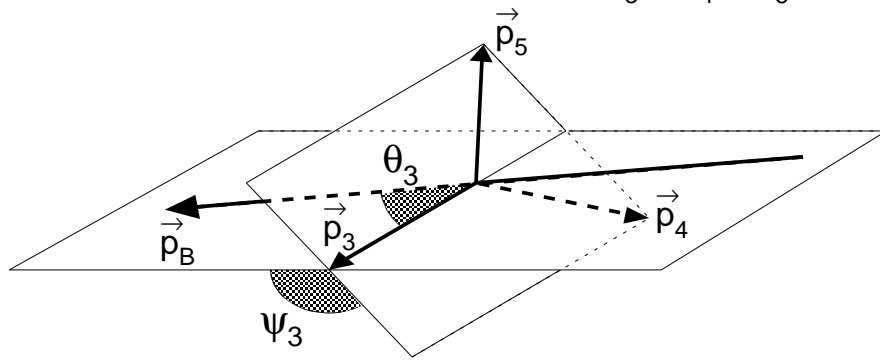


Figure 1: A sketch of the angles θ_3 and ψ_3 which are defined by the momenta \vec{p}_3 , \vec{p}_4 , \vec{p}_5 of the three jets and the proton beam (\vec{p}_B) in the three-jet center of mass frame.

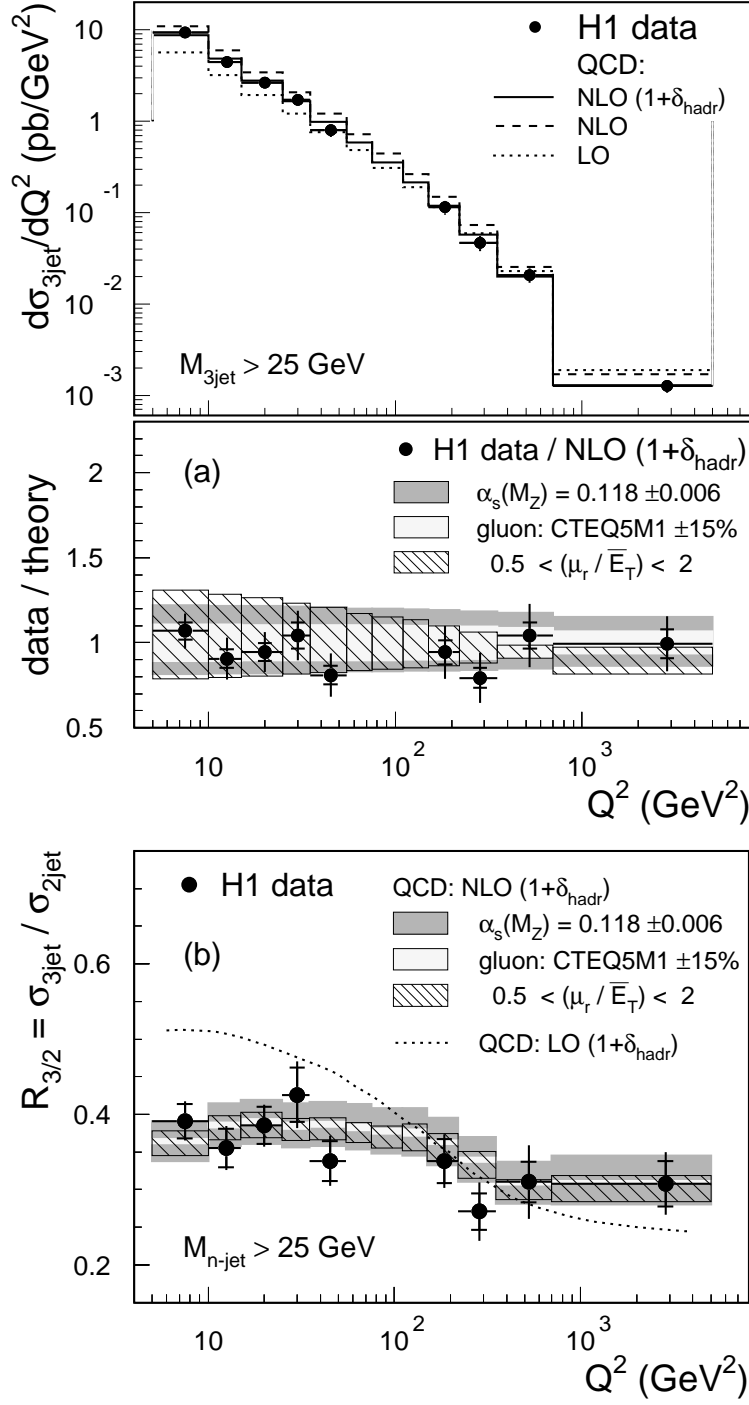


Figure 2: The inclusive three-jet cross section (a) measured as a function of the four-momentum transfer squared Q^2 . The predictions of perturbative QCD in leading order (dotted line) and in next-to-leading order with (solid line) and without hadronization corrections (dashed line) are compared to the data. Also shown is the ratio of the measured cross section and the theoretical prediction, including the effects from variations of $\alpha_s(M_Z)$, the renormalization scale μ_r and the gluon density in the proton. The ratio $R_{3/2}$ of the inclusive three-jet cross section to the inclusive dijet cross section (b) is compared to the leading order (dotted line) and the next-to-leading order calculations (central value of the light band) including hadronization corrections. The sensitivity of the NLO calculation to parameter variations is indicated as in (a). (The data at $55 < Q^2 < 100$ GeV², which are affected by the cut on θ_{positron} in eq. (3), are not included in this Figure.)

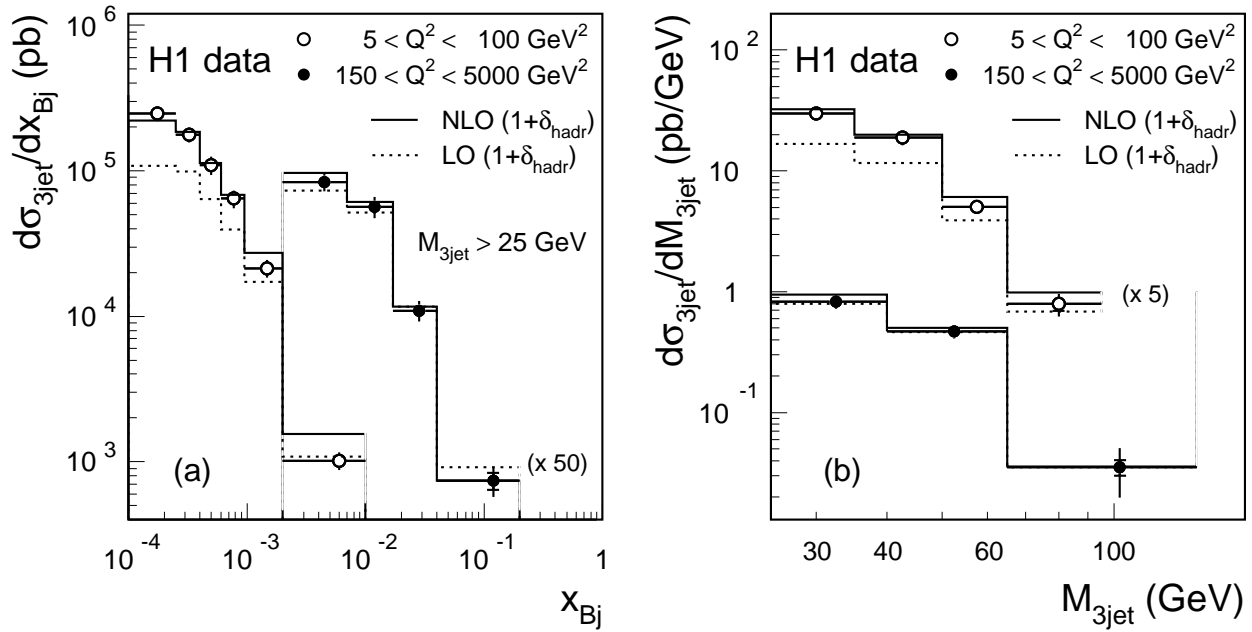


Figure 3: The inclusive three-jet cross section measured as a function of (a) the Bjorken scaling variable x_{Bj} and (b) the invariant three-jet mass $M_{3\text{jet}}$. The predictions of perturbative QCD in leading order (dotted line) and next-to-leading order (solid line) with hadronization corrections are compared to the data.

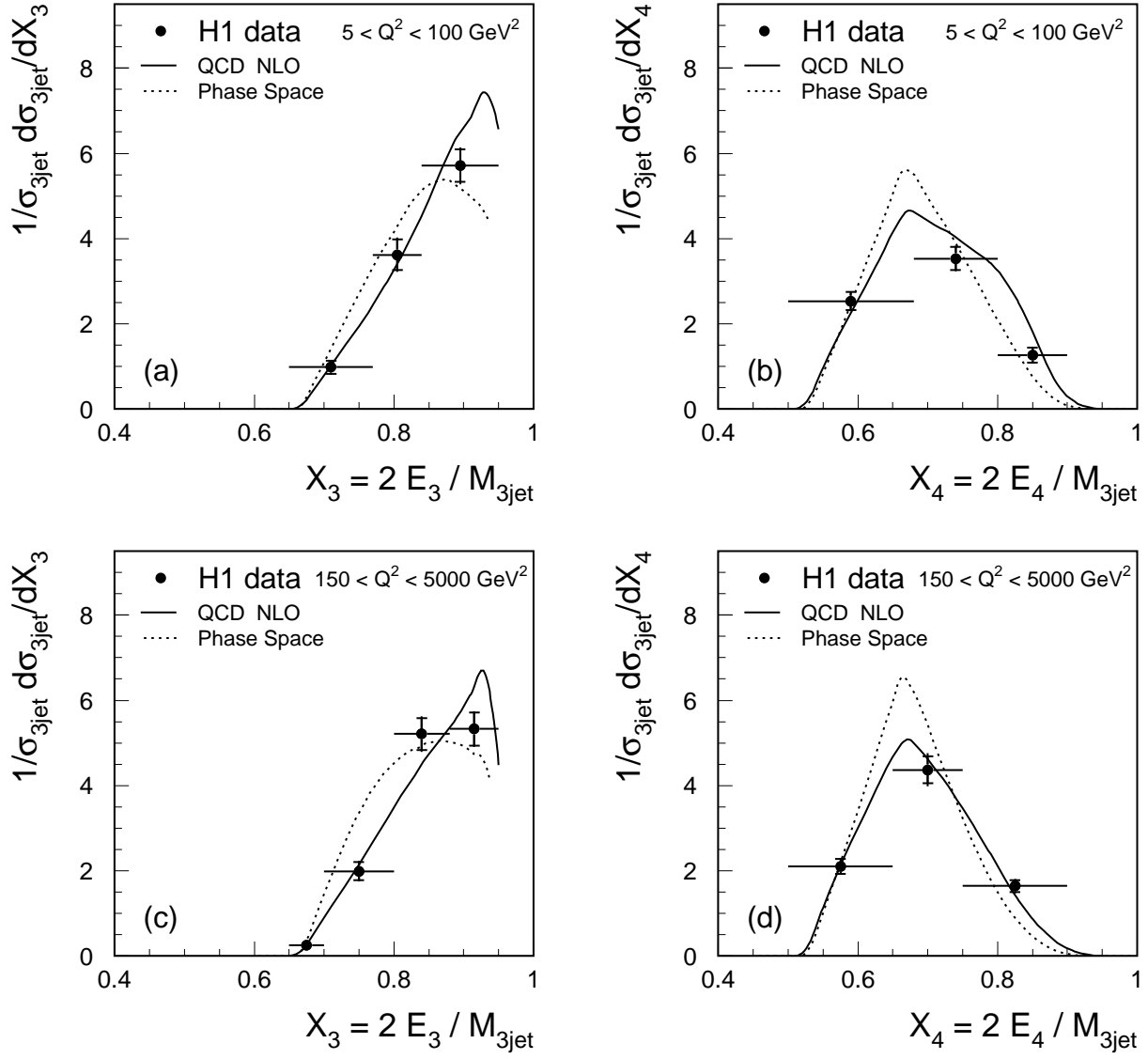


Figure 4: The distributions of the jet energy fractions X_3 (top) and X_4 (bottom) in the three-jet center-of-mass frame at low Q^2 (left) and high Q^2 (right). The data are compared to the predictions of perturbative QCD in next-to-leading order (solid line) and to a three-jet phase space model (dotted line).

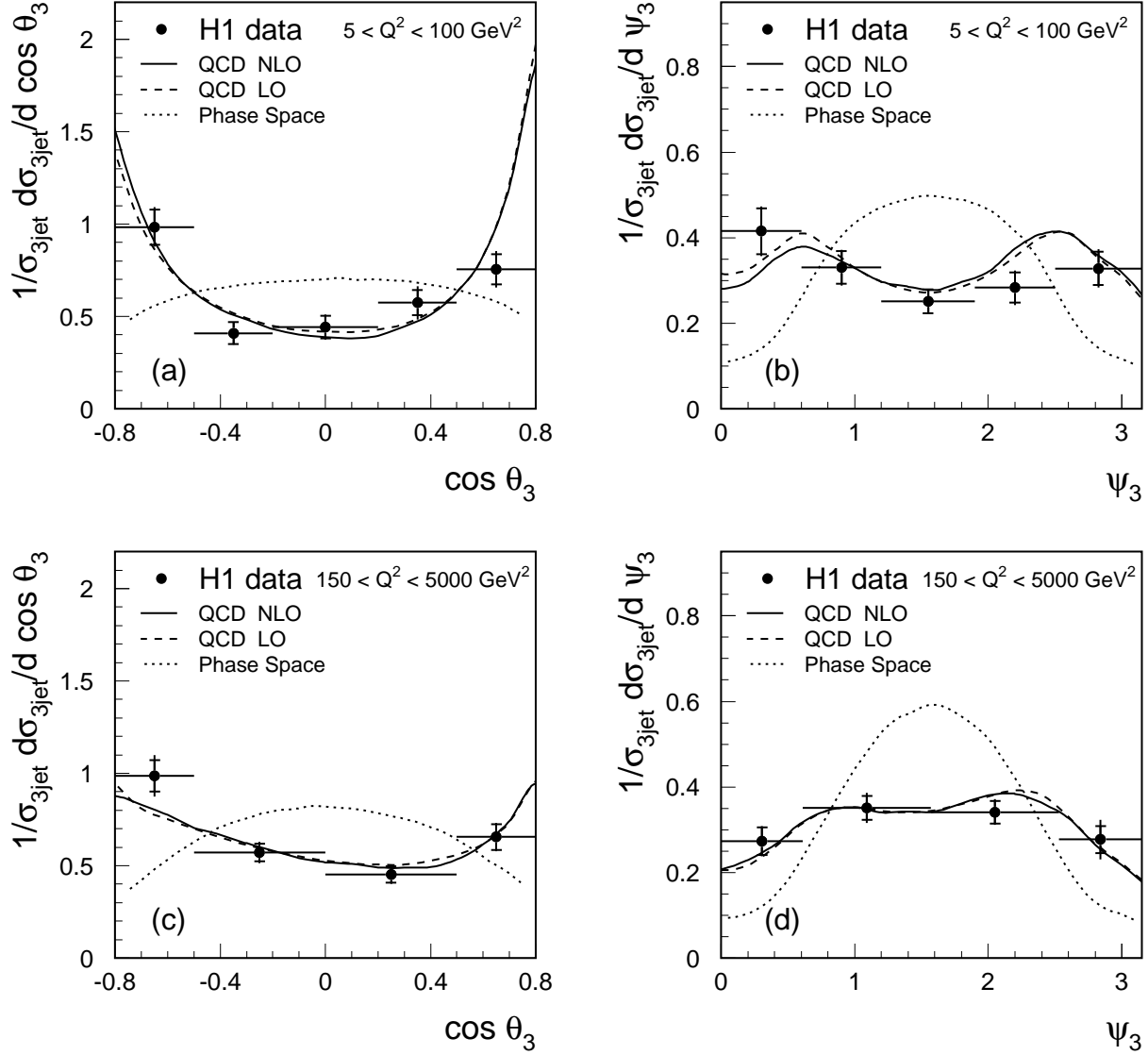


Figure 5: Distributions of $\cos \theta_3$ (top) and the angle ψ_3 (bottom) in the three-jet center-of-mass frame at low Q^2 (left) and high Q^2 (right). The data are compared to the predictions of perturbative QCD in next-to-leading order (solid line) and in leading order (dashed line) and to a three-jet phase space model (dotted line).

Q^2 [GeV ²]	$\frac{d\sigma_{3\text{jet}}}{dQ^2}$ [$\frac{\text{pb}}{\text{GeV}^2}$]	δ_{stat} [%]	δ_{syst} [%]
[5, 10]	9.33	4.8	8.4
[10, 15]	4.41	6.2	12.1
[15, 25]	2.65	5.6	11.0
[25, 35]	1.70	7.3	11.9
[35, 55]	0.802	6.7	14.4
[150, 220]	0.114	7.5	14.6
[220, 350]	0.0465	7.6	16.9
[350, 700]	0.0207	7.5	16.2
[700, 5000]	0.00128	8.6	13.8

Q^2 [GeV ²]	$R_{3/2}(Q^2)$	δ_{stat} [%]	δ_{syst} [%]
[5, 10]	0.391	5.8	3.2
[10, 15]	0.355	7.2	4.0
[15, 25]	0.385	6.4	3.5
[25, 35]	0.426	8.4	6.2
[35, 55]	0.338	7.8	6.1
[150, 220]	0.338	8.7	6.0
[220, 350]	0.271	8.9	11.2
[350, 700]	0.310	8.6	13.1
[700, 5000]	0.308	9.8	9.3

x_{Bj}	$\frac{d\sigma_{3\text{jet}}}{dx_{\text{Bj}}}$ [pb]	δ_{stat} [%]	δ_{syst} [%]
$5 < Q^2 < 100 \text{ GeV}^2$			
$[1.0, 2.5] \cdot 10^{-4}$	246507	5.6	9.6
$[2.5, 4.0] \cdot 10^{-4}$	176962	5.6	10.3
$[4.0, 6.0] \cdot 10^{-4}$	108768	6.2	12.9
$[6.0, 9.5] \cdot 10^{-4}$	64410	6.1	12.6
$[9.5, 20] \cdot 10^{-4}$	21352	5.9	12.8
$[20, 100] \cdot 10^{-4}$	1019	8.4	11.5
$150 < Q^2 < 5000 \text{ GeV}^2$			
$[2, 7] \cdot 10^{-3}$	1644	7.0	12.8
$[7, 17] \cdot 10^{-3}$	1110	6.1	16.2
$[17, 40] \cdot 10^{-3}$	214	8.8	13.8
$[40, 200] \cdot 10^{-3}$	14.5	13.5	18.3

$M_{3\text{jet}}$ [GeV]	$\frac{d\sigma_{3\text{jet}}}{dM_{3\text{jet}}}$ [$\frac{\text{pb}}{\text{GeV}}$]	δ_{stat} [%]	δ_{syst} [%]
$5 < Q^2 < 100 \text{ GeV}^2$			
[25, 35]	5.98	3.7	9.1
[35, 50]	3.76	4.0	12.2
[50, 65]	1.01	7.6	10.5
[65, 95]	0.159	12.0	18.2
$150 < Q^2 < 5000 \text{ GeV}^2$			
[25, 40]	0.833	5.5	12.3
[40, 65]	0.470	6.0	11.2
[65, 140]	0.035	14.4	41.3

X_3	$\frac{1}{\sigma_{3\text{jet}}} \frac{d\sigma_{3\text{jet}}}{dX_3}$	δ_{stat} [%]	δ_{syst} [%]
$5 < Q^2 < 100 \text{ GeV}^2$			
[0.65, 0.77]	0.98	15.9	6.7
[0.77, 0.84]	3.62	10.1	4.6
[0.84, 0.95]	5.71	6.7	3.6
$150 < Q^2 < 5000 \text{ GeV}^2$			
[0.65, 0.70]	0.25	43.1	21.7
[0.70, 0.80]	1.99	10.6	6.3
[0.80, 0.88]	5.21	7.2	3.5
[0.88, 0.95]	5.33	7.3	2.9

X_4	$\frac{1}{\sigma_{3\text{jet}}} \frac{d\sigma_{3\text{jet}}}{dX_4}$	δ_{stat} [%]	δ_{syst} [%]
$5 < Q^2 < 100 \text{ GeV}^2$			
[0.50, 0.68]	2.53	8.4	4.1
[0.68, 0.80]	3.53	7.8	3.6
[0.80, 0.9]	1.26	14.0	4.9
$150 < Q^2 < 5000 \text{ GeV}^2$			
[0.50, 0.65]	2.10	8.3	3.8
[0.65, 0.75]	4.37	7.1	5.5
[0.75, 0.90]	1.64	8.8	5.8

$\cos \theta_3$	$\frac{1}{\sigma_{3\text{jet}}} \frac{d\sigma_{3\text{jet}}}{d \cos \theta_3}$	δ_{stat} [%]	δ_{syst} [%]
$5 < Q^2 < 100 \text{ GeV}^2$			
[-0.8, -0.5]	0.984	9.6	5.0
[-0.5, -0.2]	0.409	14.5	3.3
[-0.2, 0.2]	0.442	14.1	5.8
[0.2, 0.5]	0.574	11.8	10.3
[0.5, 0.8]	0.755	10.9	7.3
$150 < Q^2 < 5000 \text{ GeV}^2$			
[-0.8, -0.5]	0.987	8.7	7.4
[-0.5, 0.0]	0.571	8.3	6.0
[0.0, 0.5]	0.451	9.8	5.4
[0.5, 0.8]	0.656	10.6	4.7

ψ_3	$\frac{1}{\sigma_{3\text{jet}}} \frac{d\sigma_{3\text{jet}}}{d\psi_3}$	δ_{stat} [%]	δ_{syst} [%]
$5 < Q^2 < 100 \text{ GeV}^2$			
[0.0, 0.6]	0.415	12.8	5.9
[0.6, 1.2]	0.330	11.6	4.8
[1.2, 1.9]	0.251	11.3	3.4
[1.9, 2.5]	0.283	12.5	6.6
[2.5, 3.15]	0.328	11.9	6.9
$150 < Q^2 < 5000 \text{ GeV}^2$			
[0.0, 0.61]	0.273	11.8	5.5
[0.61, 1.57]	0.351	8.1	6.1
[1.57, 2.53]	0.341	7.7	4.4
[2.53, 3.15]	0.277	11.3	12.3

Table 1: Results of the measurement. The values of the three-jet observables are listed together with their relative statistical and systematical uncertainties.